Simulations of seismic acquisition footprint

Joanna K. Cooper, Gary F. Margrave and Don C. Lawton

ABSTRACT

Seismic acquisition footprint generally consists of modulations in recorded amplitudes that are spatially correlated to the surface locations of sources and receivers used in a survey. These amplitude variations obscure the true reflection response of the subsurface. In this study, synthetic seismic data were produced using numerical modelling code written in MATLAB. An "exhaustive" dataset was created using a survey design incorporating dense grids of sources and receivers, chosen to guarantee fully unaliased sampling of the seismic reflections. A more commonly used survey design, involving sparser spatial sampling and resulting in forms of spatial aliasing, was created by selecting specific traces from the exhaustive survey. Both datasets were subjected to two distinct processing flows: one including stacking and poststack migration, and the other involving prestack migration. Final processed images from the exhaustive dataset were compared to those from the decimated dataset. Algorithm-dependent footprint, including edge artefacts and aperture imprints, was observed in both the exhaustive and decimated datasets. Footprint consisting of periodic amplitude variations in the interior of the surveys, similar to that observed in field data and likely produced by poor sampling, was observed in the decimated dataset. This type of footprint was also observed to vary in strength between images produced with different processing algorithms. Percent amplitude variations of up to 6% in stacks and poststack migrations, and up to 24% in prestack migrations were produced.

INTRODUCTION

Seismic acquisition footprint refers to artefacts observable in a final seismic image resulting from the acquisition geometry of the seismic survey. These artefacts generally consist of amplitude variations that coincide with source and receiver locations. Though acquisition footprint is often recognizable in seismic data, the exact nature of the effect of acquisition geometry on seismic imaging is not very well understood. Footprint artefacts have been hypothesized to be of at least two types: those arising from spatial aliasing of either coherent noise or reflections caused by inadequate spatial sampling, and those arising from inadequacies in the imaging algorithm (Margrave, 2005). To these we add a third: those related to the finite aperture of the survey.

With the purpose of increasing the understanding of the causes of acquisition footprint as well as developing strategies for reducing its effect, a seismic forward modelling study was initiated to simulate footprint artefacts observed in field data. Spatial sampling of the seismic wavefield is likely to have a central role in acquisition footprint; therefore, an effective strategy to investigate footprint is to compare seismic images produced with "exhaustive" spatial sampling to those produced with more typical source and receiver geometries. Exhaustive sampling involves very dense source and receiver lattices with source and receiver intervals small enough to adequately sample all seismic events without aliasing, while typical geometries generally involve sparser and more irregular source and receiver sampling.

The simulations were generated by the process of numerical seismic forward modelling. Kirchhoff modelling was used for 2D simulations, while a Rayleigh-Sommerfeld method was used in 3D (Margrave and Cooper, 2007). The interaction between the survey geometry and different imaging algorithms were examined by comparing results produced using "conventional" seismic processing (normal moveout correction, stack, and poststack migration) with those obtained using prestack migration algorithms. These investigations produced some preliminary conclusions, while providing groundwork for further modelling work in the examination of acquisition footprint in both 2D and 3D seismic data.

ACQUISITION FOOTPRINT

Acquisition footprint generally refers to amplitude anomalies or noise visible in seismic data that are related to the particular acquisition geometry of the survey (e.g. La Bella et al., 1998). The anomalies are commonly observed on shallow time slices in 3D volumes as modulations in amplitude that are clearly correlated to the source-receiver layout of the survey. Figure 1 shows an example of footprint visible on an amplitude map. Footprint can be present in data that has undergone a variety of processing techniques; these include unmigrated stacks, poststack and prestack migrations, and inversions. Strong acquisition footprint can have a negative effect on the interpretation of the seismic data, especially when techniques such as AVO (amplitude variation with offset) or seismic coherency are used (Marfurt et al., 1998). Removal of footprint in seismic processing can be attempted, for example by filtering, but it is difficult to ensure that true amplitude anomalies are not affected (La Bella et al., 1998).

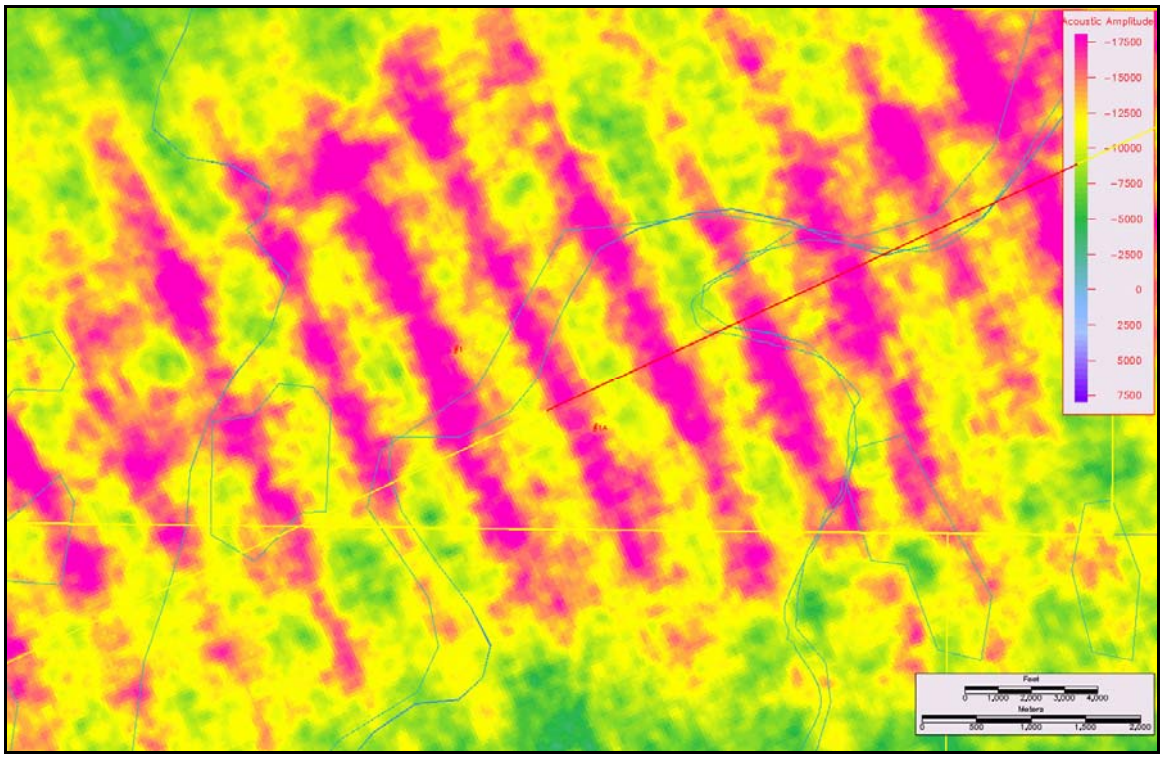

FIG. 1. Example of acquisition footprint, provided by Talisman Energy Inc.

The factors most correlated with the enhancement of footprint are irregularities in signal-to-noise ratio, fold, offset, and azimuth distributions (Cordsen et al., 2000). It is thought that a key factor in acquisition footprint is inadequate spatial sampling of the seismic wavefield, resulting in spatial aliasing (e.g. Margrave, 2005). When proper sampling is not used, the irregularities associated with the survey geometry can result in footprint. Proper or adequate sampling refers to using source and receiver sampling intervals that obey the Nyquist criterion, allowing for complete reconstruction of the continuous wavefield from the recorded samples (Vermeer, 1990). This means that the source spacing, $\Delta x_S=\Delta y_S$, and the receiver spacing, $\Delta x_R=\Delta y_R$, must obey

$$\Delta x_S \le \frac{1}{2|k_S|_{MAX}} = \frac{v_{MIN}}{2 f_{MAX}}, \text{ and} \tag{1}$$

$$\Delta x_R \le \frac{1}{2|k_R|_{MAX}} = \frac{v_{MIN}}{2 f_{MAX}}, \tag{2}$$

where k_S and k_R are the source and receiver wavenumbers, v_{MIN} is the minimum horizontal apparent velocity, and f_{MAX} is the maximum frequency in the data (Vermeer, 1990). The relationship between k_{MAX}, v_{MIN}, and f_{MAX} comes from the boundary between the propagation and evanescent regions of f-k space, a line with slope $1/v_{MIN}$.

Generally, using these criteria to determine sampling intervals used in the field results in prohibitively expensive survey designs. The best way to produce artefact-free data without resorting to the fundamental "exhaustive" sampling interval is currently a topic of research. Different acquisition geometries, for example Vermeer's (1998) symmetric sampling, have been proposed as optimal for reducing footprint because of their ability to sample the continuous wavefield in a more acceptable way.

Footprint artefacts are also product of the migration algorithm used to create the final seismic images (Margrave, 2005). Irregularities and aliased energy in the data input to migration tend to result in noise in the migrated output. Figure 2 is a simple example of this effect, from Bancroft (2006), showing the f-k spectra of spatially aliased data before and after migration. The aliased energy is improperly migrated. It can be shown (e.g. Vermeer, 1990; Margrave, 2005) that the wavenumber content of a stacked section comes equally from both source and receiver wavenumbers, i.e.

$$k_M = k_S + k_R, \tag{3}$$

where k_M is the midpoint wavenumber. This suggests that aliasing in either source or receiver sampling domains, or both, would result in aliased contributions to the final seismic image.

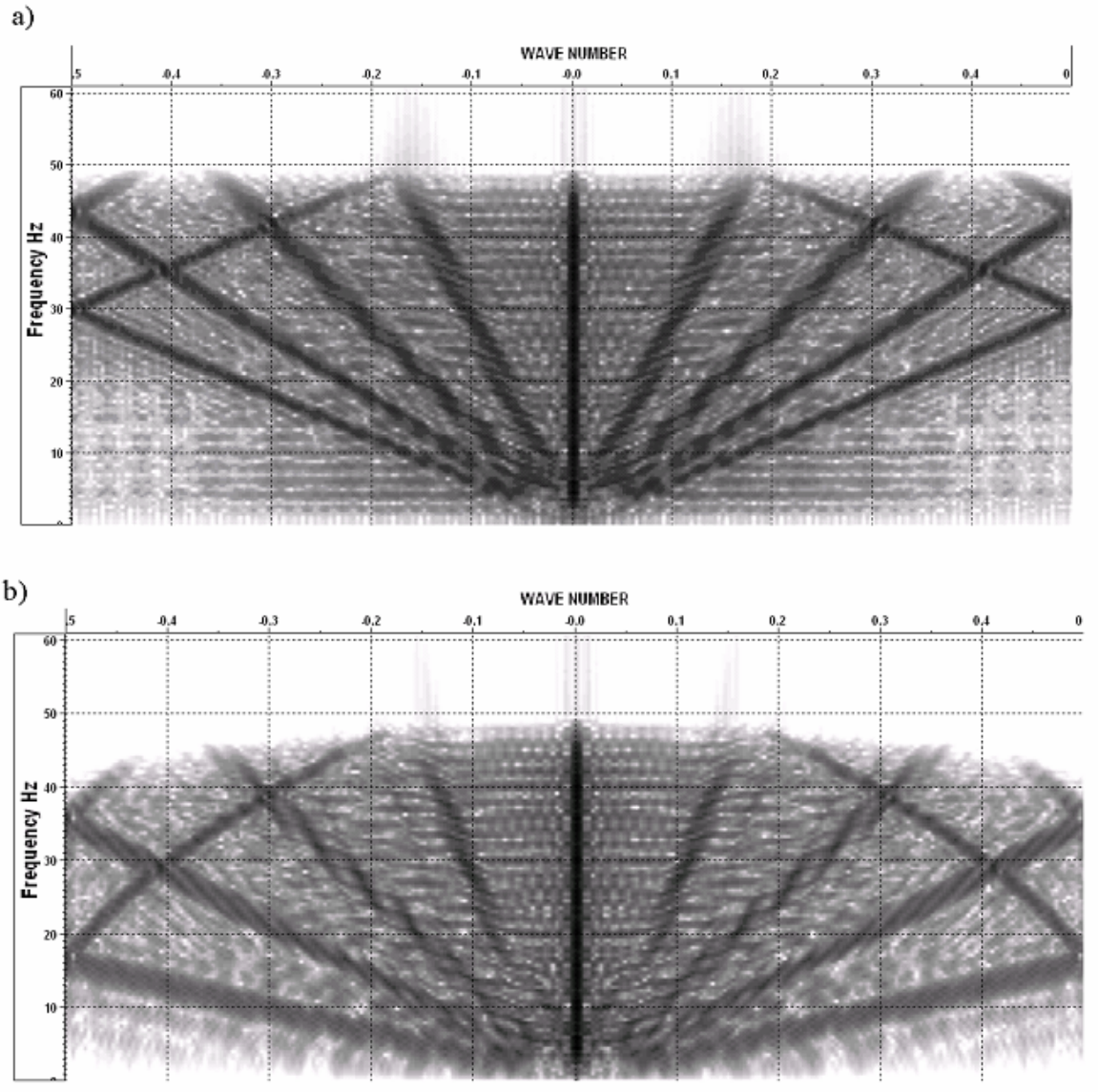

FIG. 2. The f-k spectra of spatially aliased data a) before migration, and b) after migration, modified from Bancroft (2006).

Though many different survey designs are used in practise, typical land 3D surveys (e.g. Figure 3) involve source and receiver sampling such that at least two of the five prestack dimensions (x_S, y_S, x_R, y_R, and t) are aliased. Along the source and receiver lines (the x_S and y_R directions in Figure 3) the sampling is good, but in the direction perpendicular to the source lines (the y_S direction) the source sampling is poor, and in the direction perpendicular to the receiver lines (the x_R direction) the receiver sampling is poor. Processing of the data, during which we map the five sampled dimensions (x_S, y_S, x_R, y_R, and t) to three dimensions (x, y, and z), generally produces good images of the subsurface, suggesting that to some degree we can get away with these violations of the sampling theorem. Weighting schemes and regularization methods are likely key to this process, as is the fact that we compress two of the five data dimensions in the course of imaging. Footprint artefacts, though, may result because processing is unable to

completely overcome the problems introduced by poor sampling. In addition, inadequacies in processing algorithms may generate artefacts.

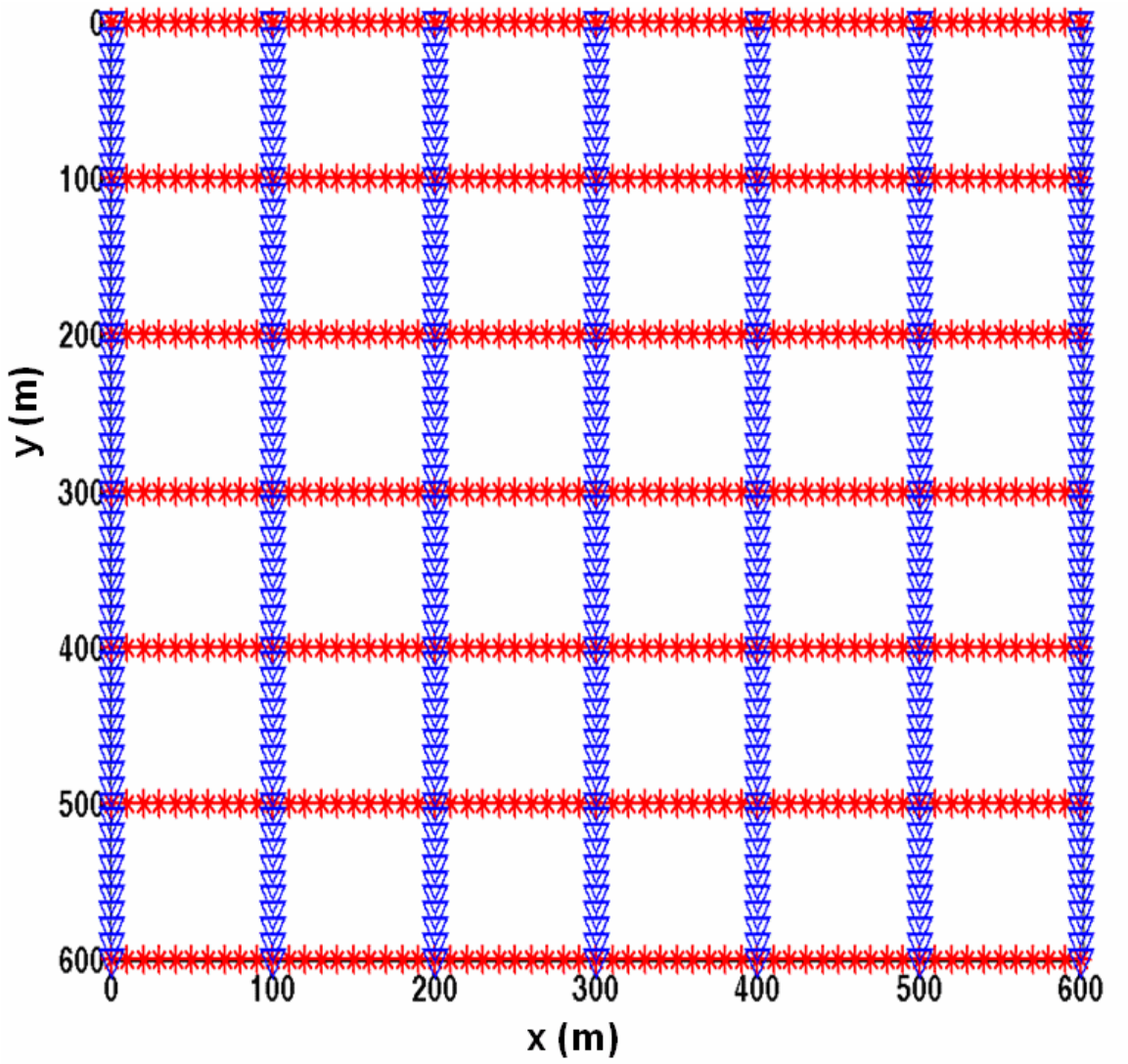

FIG. 3. Typical 3D survey geometry. Source positions are red and receiver positions are blue.

2D FOOTPRINT SIMULATION

The 2D example described here illustrates acquisition footprint related to prestack migration. The simulation is similar to that published by Cary (2007). However, the results of our simulation support a relationship between the presence of footprint and aliased spatial sampling. The simulation used a 2D Kirchhoff modelling algorithm implemented in MATLAB following the description given by Shearer (1999). The MATLAB function produces a synthetic shot record with the seismic response from a single reflector using the input velocity-depth profile of the overburden, spatial positions of the source and receivers, and reflection coefficient of the reflector as a function of lateral position. Following Huygens' principle, the seismic trace recorded at each receiver in the shot record is calculated as a summation of diffractions produced by all points on the reflector. The arrival time for the contribution from each point on the

reflector is calculated by raytracing from the reflector to each source and receiver. The amplitude of each contribution is scaled by factors related to geometrical spreading and raypath obliquity. The modelling technique includes effects such as scattering, diffraction, and rays that do not obey Snell's law of reflection.

The velocity model used for the simulation is described by Margrave and Cooper (2007). It is a v(z) model with velocities ranging from 1200 m/s in the near surface, to 3000 m/s at depths greater than 190 m. The model described by Margrave and Cooper includes 3 reflecting interfaces; for this 2D simulation only the channel reflector was included in the model. The particular 2D vertical cross section through the channel reflector used for the simulations has the channel located in the middle of the section, from x=175-225 m. The reflection coefficient associated with the channel is negative, while the rest of the reflector has a positive reflection coefficient. The wavelet was defined using the *filtspec* function from the CREWES MATLAB toolbox, with a frequency specification of [5 10 100 125] Hz. Shot records were created using different source positions, and were combined to produce stacked sections. The processing flow involved prestack Kirchhoff shot record migration then stacking of the migrated shot records. A suite of sections was created with shot spacings ranging from 5 m to 200 m. The receiver positions remained the same, located from x=2.5-397.5 m in 5 m intervals. The resulting images simulated exhaustive and shot-reduced survey geometries, and allowed the effect of sparse source sampling to be examined.

Figure 4 shows the sections produced using prestack migration, for shot spacings of 5, 10, 25, 50, 100, and 200 m. The sections produced using spacings of 5 m and 10 m are essentially identical; the sections produced using spacings of 50, 100, and 200 m contain artefacts; the section produced using a spacing of 25 m appears to also contain some faint artefacts. The artefacts seem to consist of residual "migration wavefronts", which is consistent with observations by Cary (2007). These artefacts would cause amplitude variations in reflection events occurring above the modelled reflector, resulting in acquisition footprint.

Because the receiver spacing was constant, the shot records (common shot gathers) produced for a given shot location are identical for all shot spacings. However, the common receiver gathers are different for the different shot spacings, with successively fewer traces as the shot interval increases. Figure 5 shows the f-k spectra for the common receiver gathers for the receiver located at x=200 m. Because these are common receiver gathers, the wavenumber axis is k_S, the shot wavenumber.

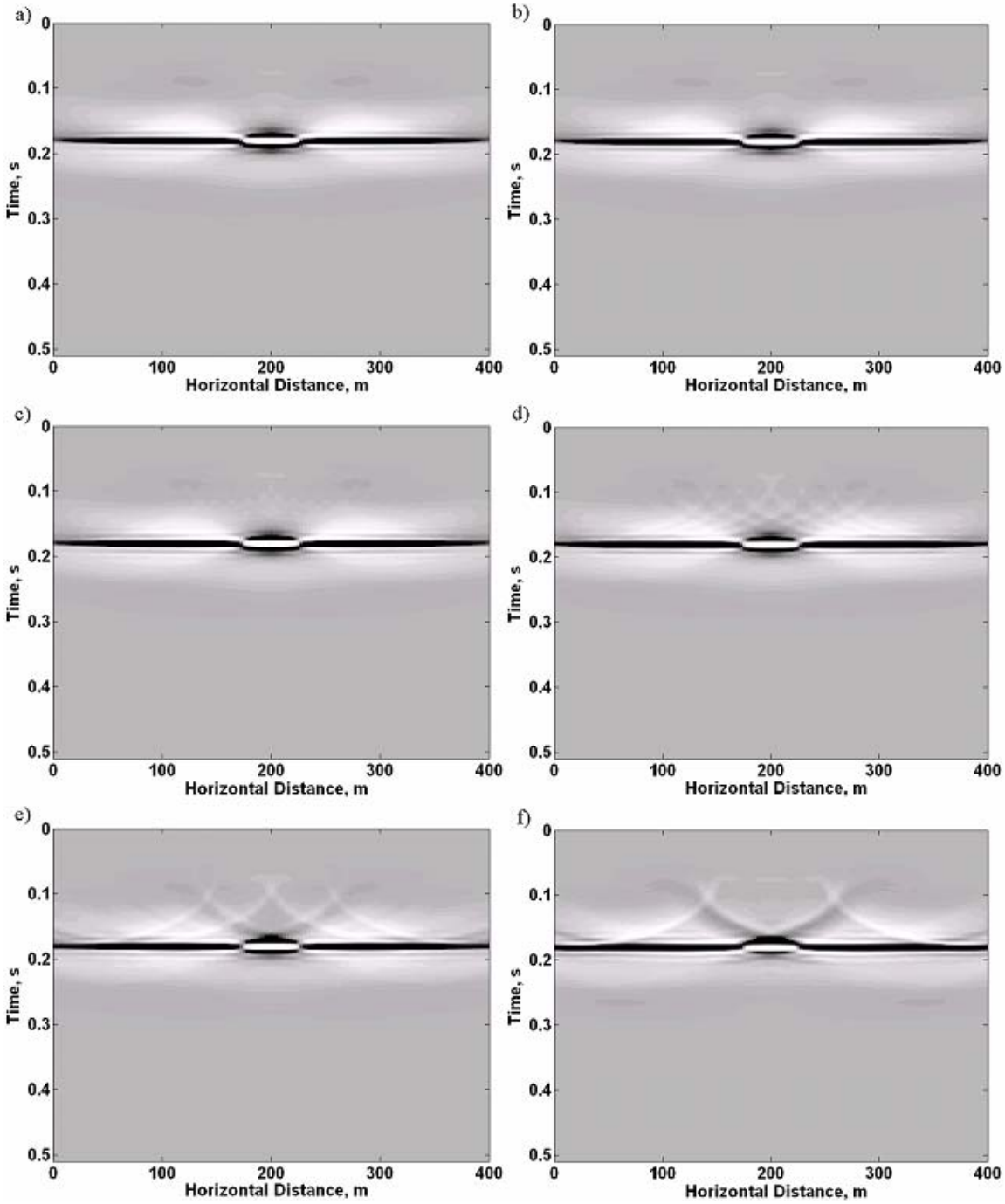

FIG. 4. Prestack migrated sections created using a) 5 m, b) 10 m, c) 25 m, d) 50 m, e) 100 m, and f) 200 m shot intervals.

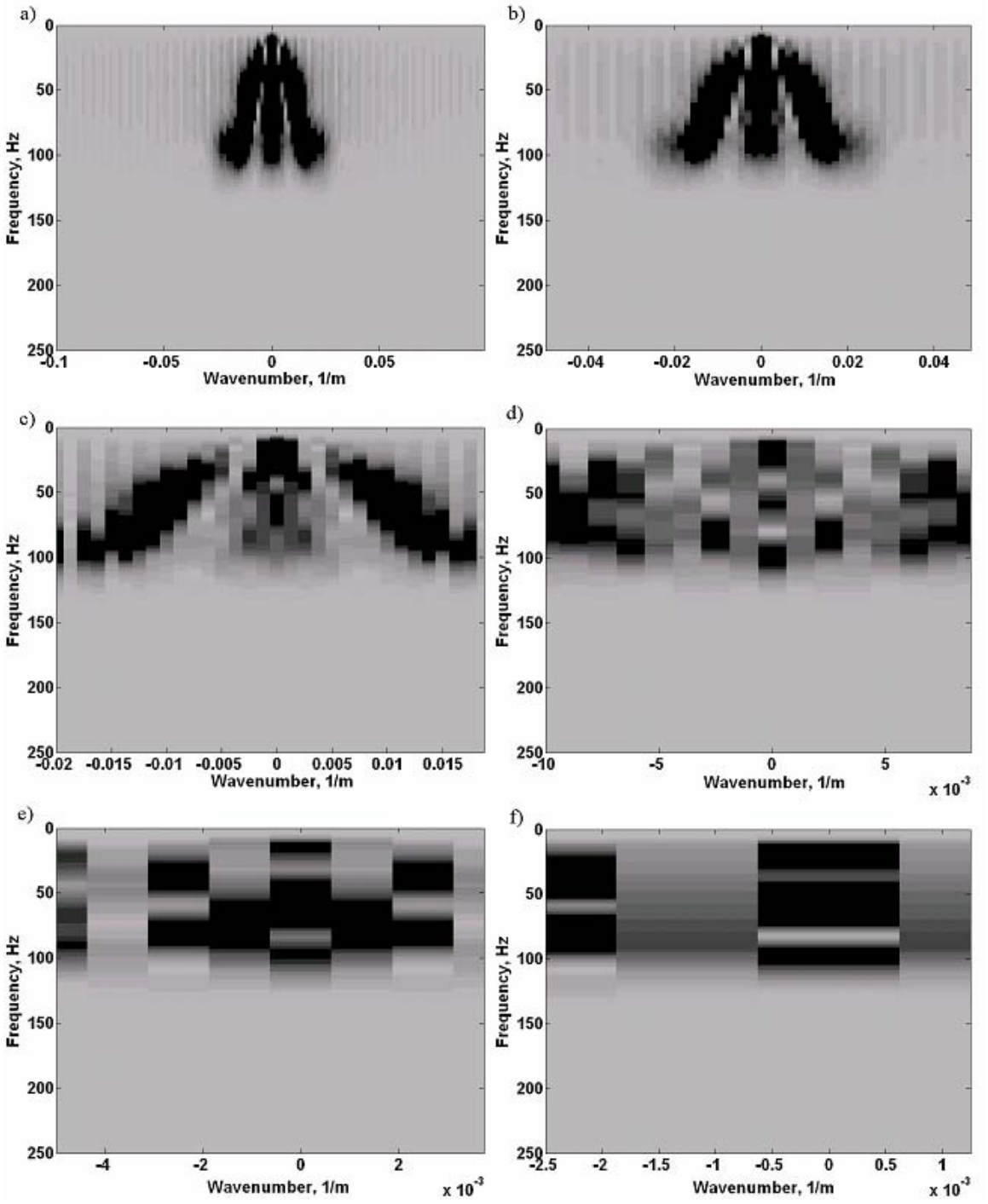

FIG. 5. The f-k spectra of common receiver gathers created using a) 5 m, b) 10 m, c) 25 m, d) 50 m, e) 100 m, and f) 200 m shot intervals.

The f-k spectra show that for shot spacings of 5 m and 10 m, the common receiver gathers are unaliased. The 25 m spacing produces a saturated spectrum, on the verge of aliasing. For the shot spacings of 50, 100, and 200 m, the f-k spectra show pronounced aliasing of the shot wavenumbers. We observe that (1) when aliasing is not present, residual migration wavefronts do not appear, (2) when the sampling is such that the

spectrum is just barely beginning to alias (25 m shot spacing), artefacts begin to appear in the prestack migrated section, and (3) when aliasing is present, residual migration wavefronts are present. The onset of footprint artefacts in the migrated stacks coinciding with the onset of aliasing in the common receiver gathers is consistent with the hypothesis that the aliased source wavenumbers are causing the artefacts, though these results do not provide definitive proof of this concept. If the source interval was kept constant and the receiver spacing increased, it is likely that the same results would be produced. Increasing both the source and receiver sampling intervals would likely result in more prominent artefacts.

The results of these tests show that for the particular reflection modelled, the exhaustive sampling interval of 5 m was excessively small. This is because the exhaustive sampling interval was calculated from v_{MIN} in the geological model, but only the reflection from the interface at the channel level was modelled. As a result, the datasets produced that simulated shot spacings of 5, 10, and 25 m were all adequate to prevent aliasing. However, if the shallower reflections or direct arrivals were included in the model the 5 m spacing would be required to prevent aliasing.

3D FOOTPRINT SIMULATIONS

To investigate acquisition footprint in its common form of amplitude modulations on time or depth slices from 3D seismic volumes, simulations of an exhaustive 3D survey were performed using Rayleigh-Sommerfeld modelling. See Margrave and Cooper (2007) for a detailed description of the modelling method and the exhaustive dataset. The method produces a shot record by initiating a source with a given spectrum and downward continuing the wavefield to the reflector by phase-shifting. Then, the wavefield is multiplied by a reflection coefficient which is a function of x and y. Finally the wavefield is propagated back to the surface. The method includes spreading loss but not multiples, direct arrivals, or noise. The speed of Rayleigh-Sommerfeld modelling compared to Kirchhoff modelling in 3D prompted its use in this study.

The exhaustive dataset was produced using shot, receiver, shot line, and receiver line spacings of 10 m. Figure 6a shows the geometry. The survey involves 1681 shots, with 1681 receivers live per shot, which required three days to model. The spectrum of the wavelet used in the modelling and the velocities of the layers in the model are described by Margrave and Cooper (2007). With these frequencies and velocities, the exhaustive sampling interval of 10 m resulted in no aliasing of reflections in shot or receiver domains. Figure 7a shows the f-k spectrum of a slice taken at y=200 m through a shot record for a source position at (0 m, 200 m); the spectrum shows no aliasing.

In order to produce datasets simulating more typical field acquisition geometries, several decimations of the exhaustive dataset were produced. One of these decimated datasets will be discussed here. As shown in Figure 6b, the decimated survey geometry is an orthogonal survey design typical of many land 3D surveys. The source lines run parallel to the y-axis and the receiver lines run parallel to the x-axis. The source line and receiver line spacings are 80 m, though the source and receiver spacings within lines remain equal to the exhaustive sampling interval, 10 m. This results in aliasing of shot wavenumbers in the x-direction and of receiver wavenumbers in the y-direction. Figure

7b shows the f-k spectrum for the y=200 m slice through a shot record from the decimated survey in the same position as that shown in Figure 7a from the exhaustive survey. Figure 7b clearly illustrates the aliasing occurring in the x-direction, orthogonal to the shot line direction.

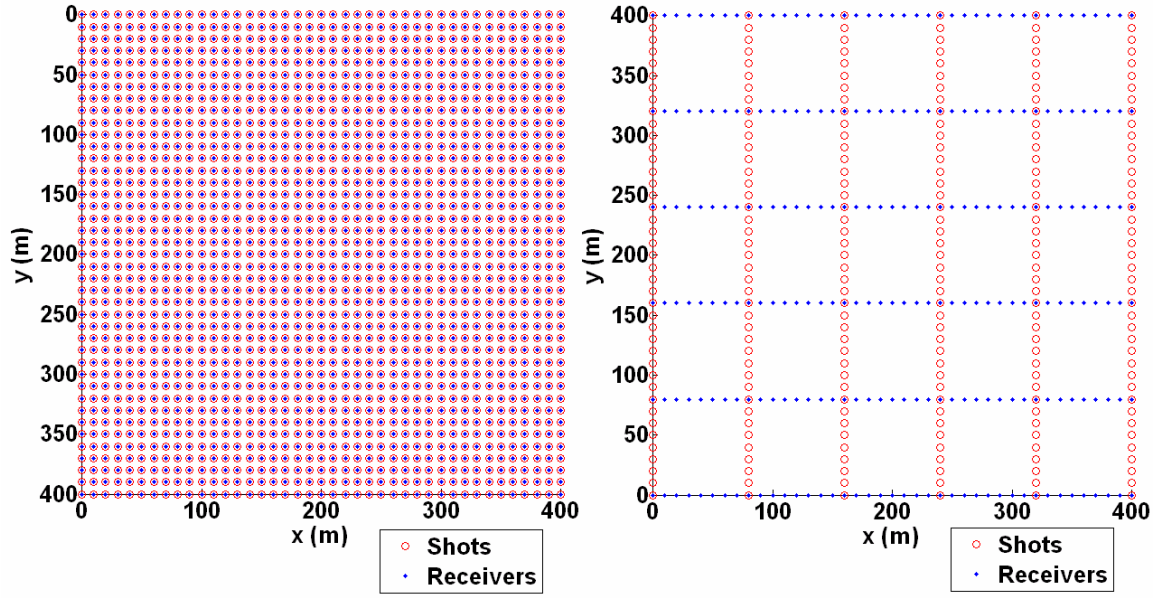

FIG.6. Geometry of a) the exhaustive survey and b) the decimated survey.

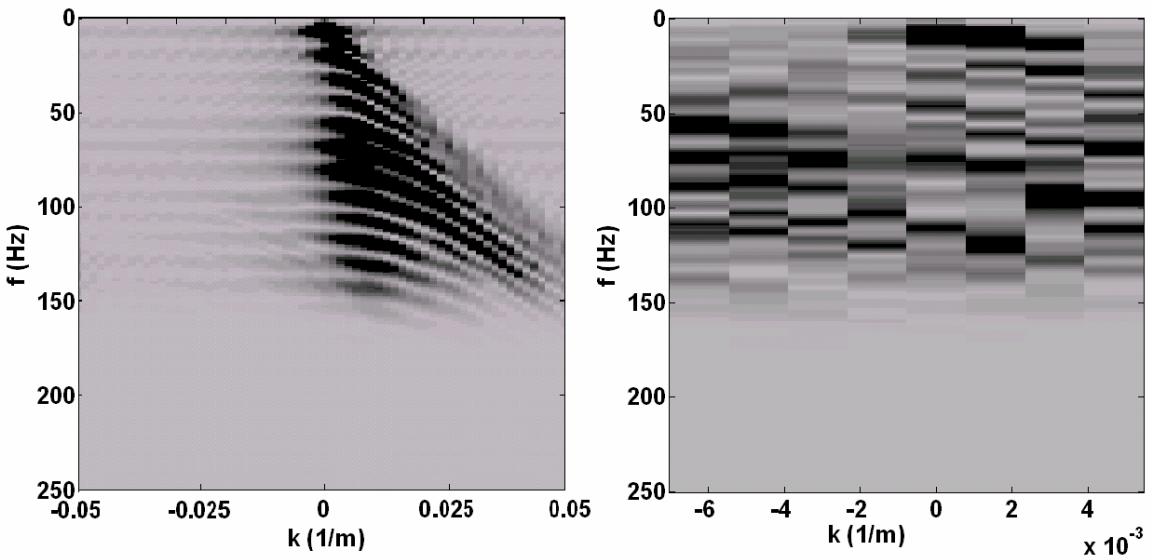

FIG. 7. The f-k spectra for slices at y=200 m through 3D shot records from a) the exhaustive dataset and b) the decimated dataset, produced by a source at (0 m, 200 m).

Both the exhaustive and decimated datasets were subjected to several processing techniques, in order to examine the interaction between sampling and various imaging algorithms. In all cases, exact model velocities were used and deconvolution was not applied. Table 1 summarizes the different flows. Processing at the University of Calgary was performed in MATLAB, producing a CMP stack, a Kirchhoff poststack migration of

that stack, and a Kirchhoff prestack migration. The prestack migration algorithm (*kirk_shot3Dfz* in the CREWES MATLAB toolbox) is a Kirchhoff shot record migration incorporating Bleistein shot weights (Bleistein, et al., 2001). The algorithm is a prestack time migration that produces images at depth levels specified by the user. Time shifts involved in the summation over traveltime paths are performed by frequency-domain phase shifts applied to slices of data around each event. For this study, a 60° scattering angle limit was used. The poststack migration algorithm (*kirk_stack3D* in the CREWES MATLAB toolbox) is an extension of the shot record migration algorithm to the case of coincident source and receiver positions.

Two additional prestack migration algorithms were applied to the data by industrial partners in this study. Algorithm A is a Kirchhoff common-offset-vector migration which involves the formation of common-offset-vector (COV) volumes, each containing traces with a limited range of inline and crossline offsets. Partial stacking may be involved in forming these COV volumes. Each COV volume is migrated separately, also using weights prescribed in Bleistein et al. (2001); the final image is formed by stacking the migrated COV volumes. Algorithm B is a Kirchhoff common-offset migration, which involves the formation of common-offset (CO) volumes, each containing traces with a limited range of absolute source-receiver offsets. These CO volumes are migrated separately using empirical weights inspired by Kirchhoff poststack migration theory. Bleistein et al. (2001) weights can also be implemented in this algorithm; however, for this dataset the difference in the stacked images produced using Bleistein weights and these empirical weights was negligible. Within a single CO volume migration the offset-range limited fold is computed for each input trace, and the trace is weighted by the inverse of this fold prior to migration. As in the COV migration case, the final image is formed by stacking the migrated CO volumes.

Table 1. Summary of processing methods applied to the model data.

Method	Description
UofC Stack	Deterministic gain, NMO correction, mute, stacking
UofC Poststack Migration	Kirchhoff poststack migration of UofC Stack, using Bleistein shot weights for zero offset
UofC Prestack Migration	Kirchhoff shot record migration using Bleistein shot weights, mute, stacking of migrated shots
Prestack Migration A	Formation of common-offset-vector volumes, Kirchhoff migration, stacking of migrated COV volumes
Prestack Migration B	Formation of common-offset volumes, weighting by offset-range limited fold, Kirchhoff migration, stacking of migrated CO volumes

Figures 8-12 show time and depth slices from processed volumes produced by applying the five processing methods. Each figure contains the slices corresponding to the appropriate time or depth of the three reflectors in the model from both the exhaustive and decimated datasets. All slices are scaled individually to their maximum and minimum amplitudes and are plotted using a linear colour scale.

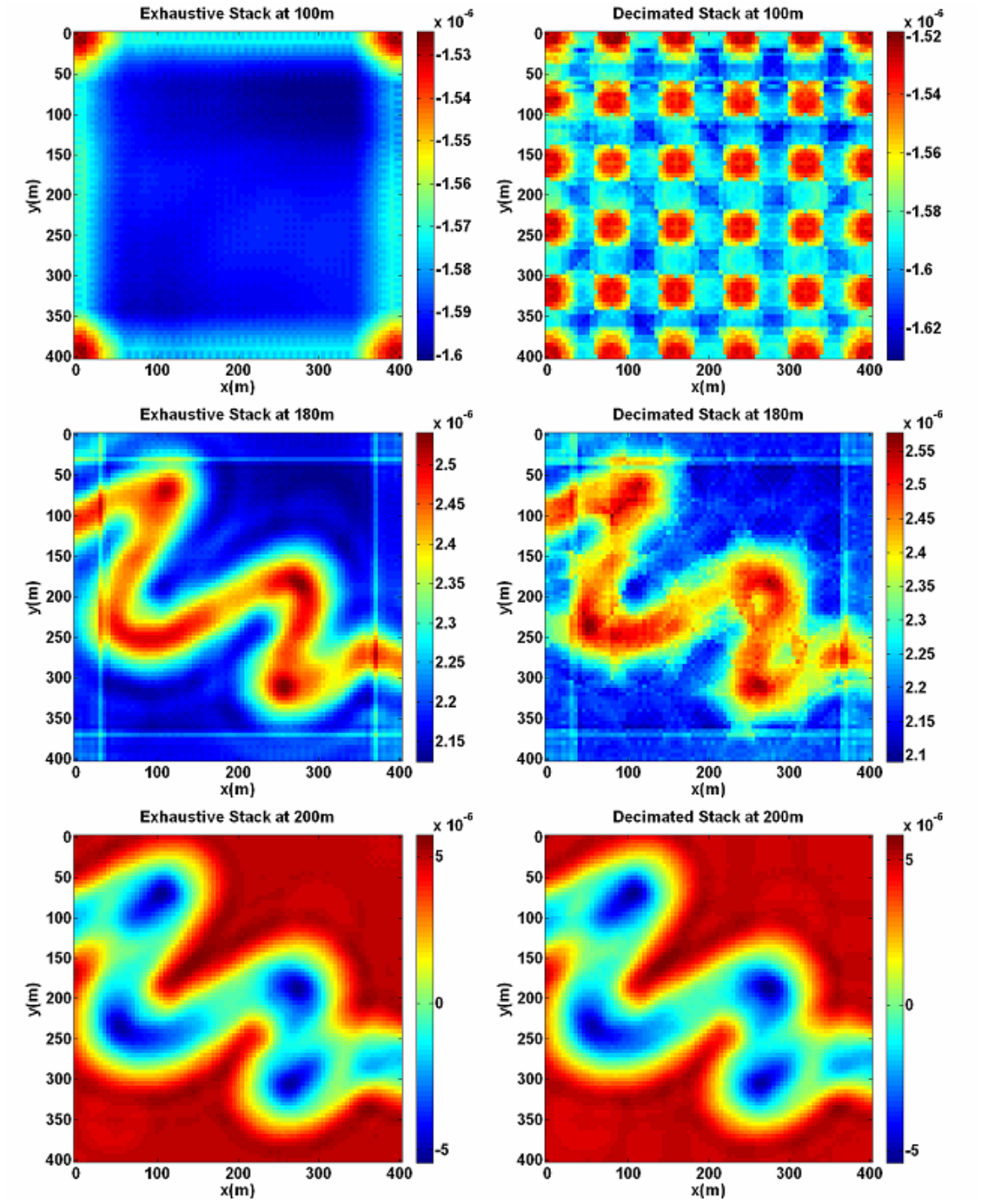

FIG. 8. Time slices from UofC stacks for the exhaustive and decimated datasets.

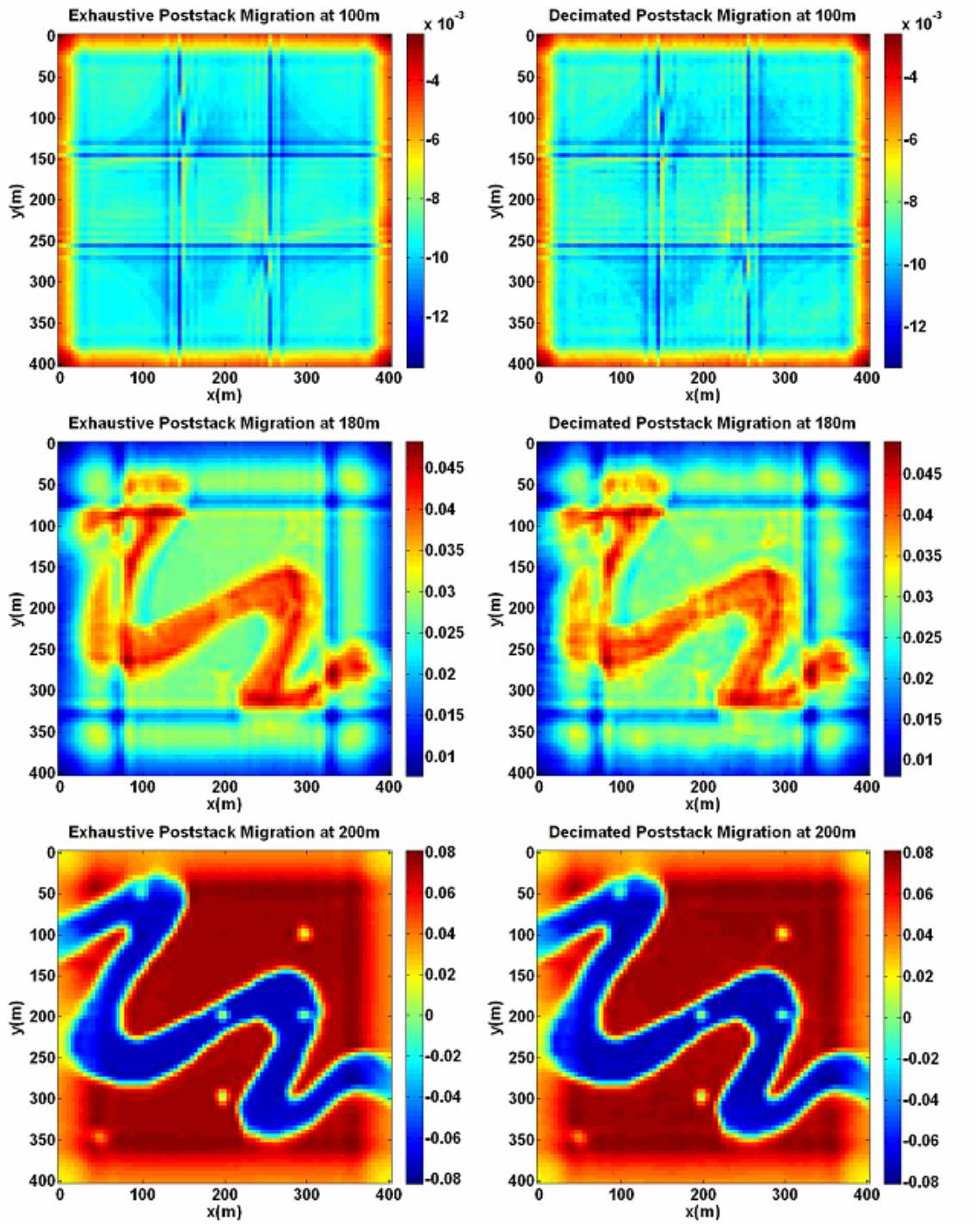

FIG. 9. Depth slices from UofC poststack migrations for the exhaustive and decimated datasets.

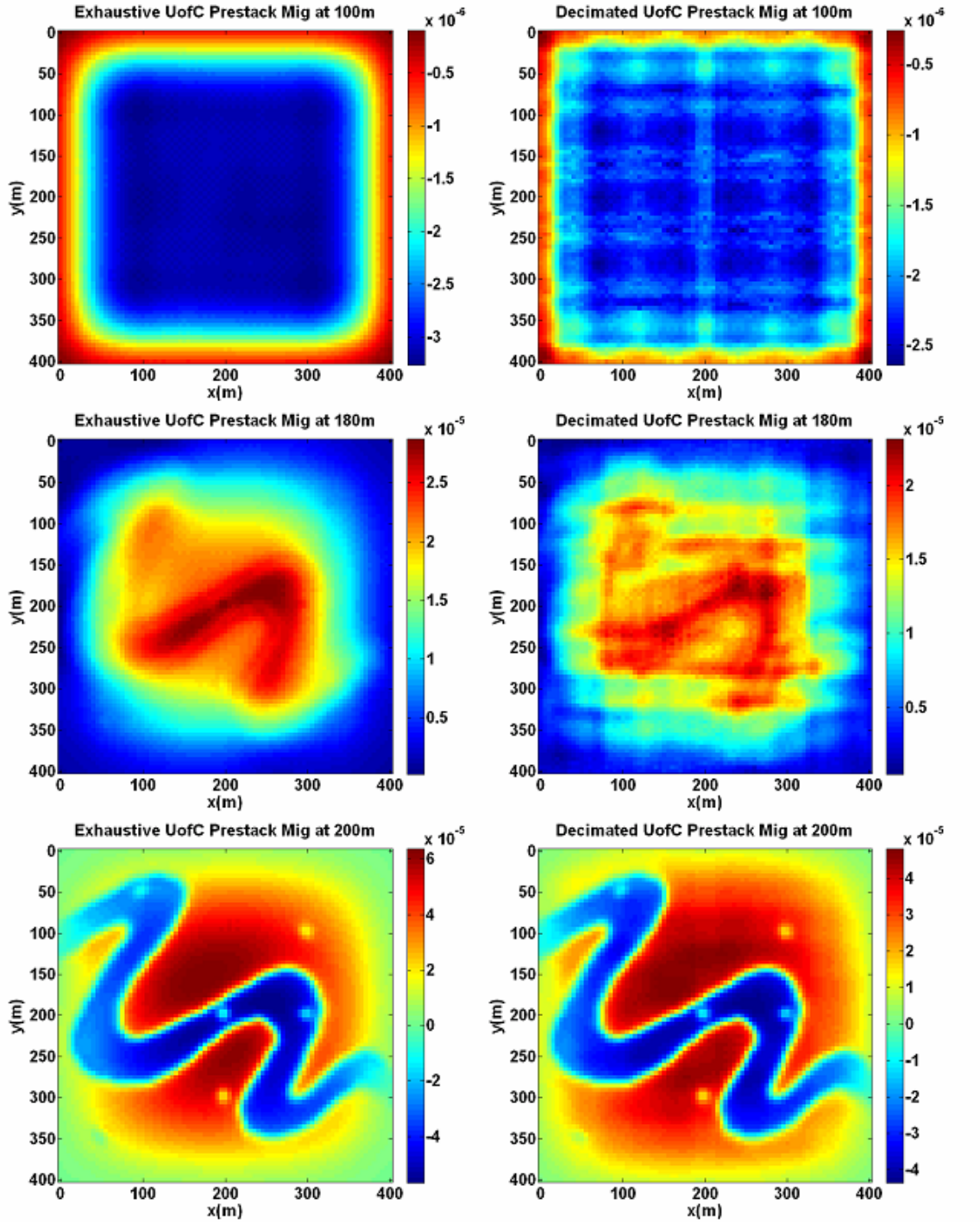

FIG. 10. Depth slices from UofC prestack migrations for the exhaustive and decimated datasets.

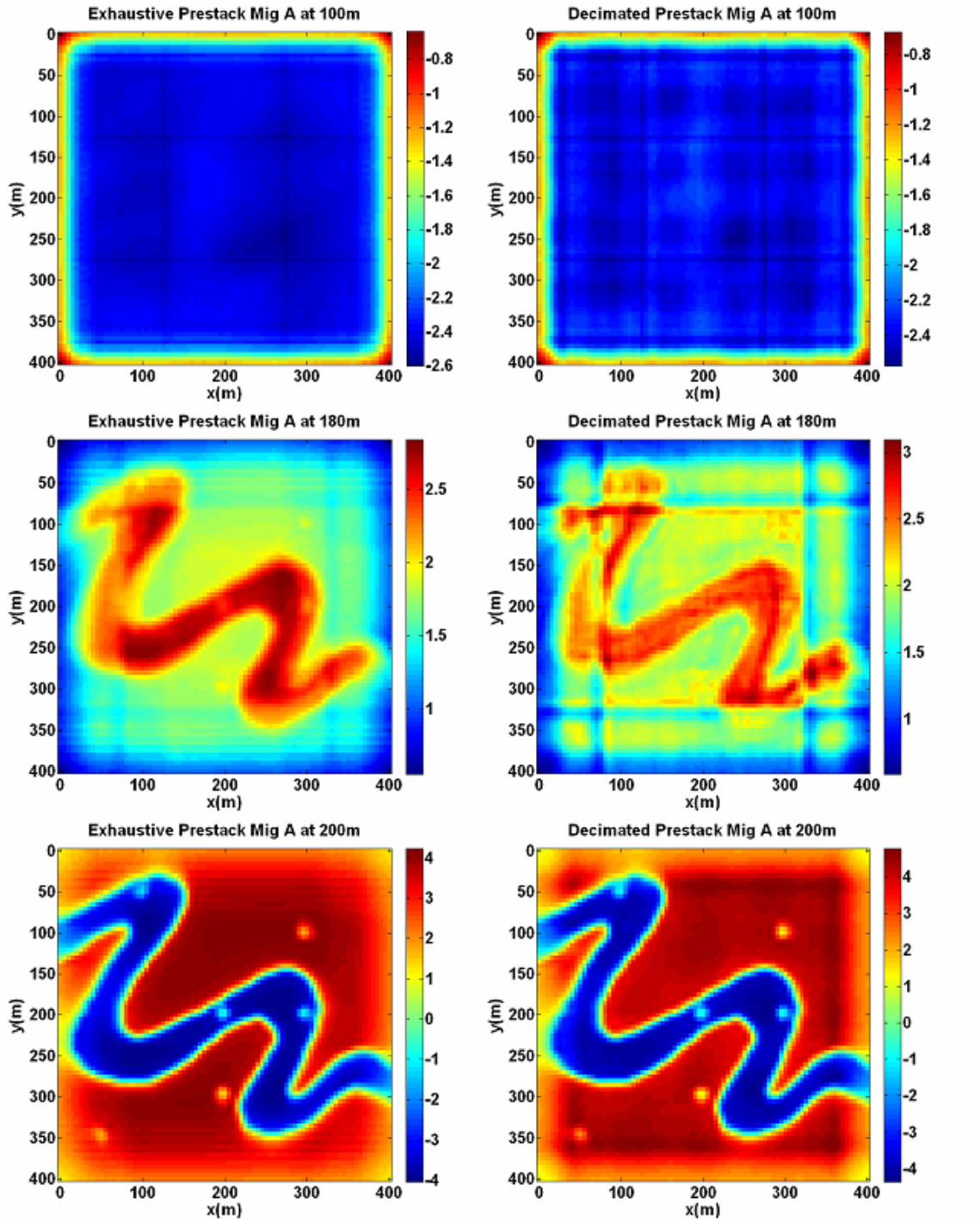

FIG. 11. Time slices from Algorithm A prestack migrations for the exhaustive and decimated datasets.

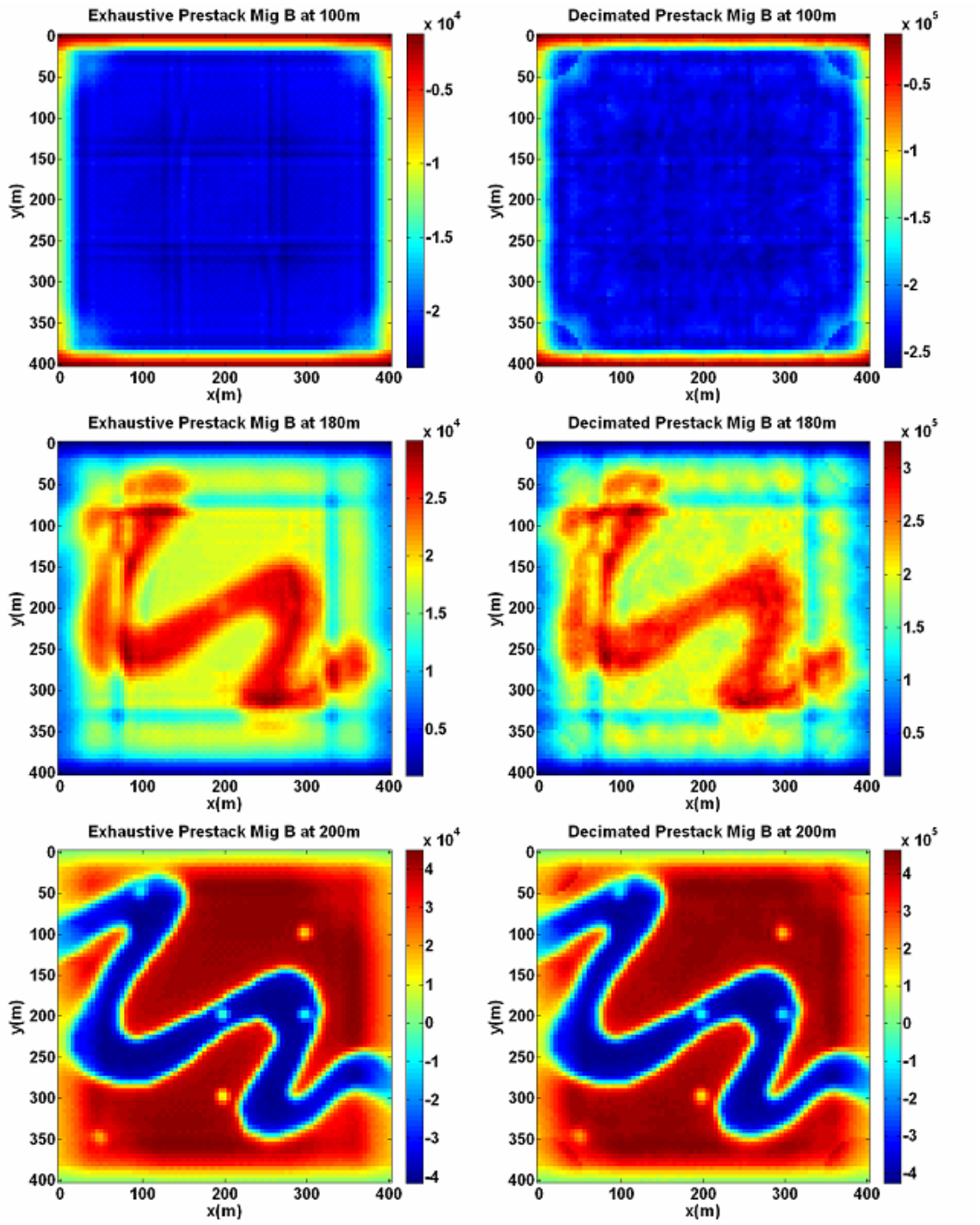

FIG. 12. Time slices from Algorithm B prestack migrations for the exhaustive and decimated datasets.

DISCUSSION

The processed results from the exhaustive dataset show high-quality images of the reflectivity structure of the geological model. Except for the edges of the survey, images of the shallow featureless reflector generally contain very uniform amplitudes. The migrated images of the channel show well-defined boundaries and crisp point scatterers.

The images of the 180 m featureless reflector show a channel imprint due to the non-causality of the wavelet used in modelling, as discussed by Margrave and Cooper (2007). The noticeable artefacts in the processed exhaustive dataset are edge artefacts on shallow reflectors, especially on the UofC poststack migration (Figure 9), caused by a lack of absorbing boundaries or edge tapering in the migration. In Figure 12, edge artefacts on the 180 m reflector are also evident; again, their presence is due to a lack of edge tapering in the migration (in this case, to save run time). The UofC prestack migration (Figure 10) exhibits a strong aperture imprint. We define footprint as any features present in an image of the featureless reflector; by this definition there is footprint in the exhaustive dataset from finite source-receiver coverage on the surface and from inadequacies in the processing algorithms. However, the more typical footprint observed in field data is observed in images from the decimated dataset. This footprint consists of periodic amplitude variations in the interior of the survey; these artefacts are also algorithm dependent. However, with each slice scaled independently it is somewhat difficult to visually assess the severity of the footprint artefacts. We decided to quantify the footprint as a percent variation in amplitude between the decimated slice and exhaustive slice. The percent variations were calculated by first scaling the decimated slice by a constant. The constant, c, is calculated by least squares; the sum of the squared point-by-point differences between the exhaustive slice and (c*decimated slice) is minimized. Then the result of the point-by-point difference (exhaustive slice – c*decimated slice) is divided by the maximum absolute amplitude of the exhaustive slice. Multiplication by 100% produces a measure of percent variation. The results of this measure are shown in Figures 13-15 for the shallow featureless reflector and the channel reflector.

Since a stack is essentially an average of traces over offset in a common midpoint gather, trivially there will be no footprint if all traces are the same. However, even in the case of a horizontal featureless reflector, NMO corrected traces will exhibit variations due to NMO stretch; in field data, additional differences will occur because of noise, multiples, velocity errors, AVO, and imperfect gain, among other factors. Still, if a survey involves homogeneous offset and fold distributions in all bins, footprint will not be observed since the same traces are being averaged; this case is represented by the exhaustive dataset. However, if traces show variation with offset and the survey involves large changes in the distributions of offset and fold then footprint is likely to occur; this case is represented by the decimated dataset. As shown in Figure 13, variations in amplitude of up to 4% on the featureless reflector and up to 6% at the channel were produced. The amplitude variations are highly regular on the featureless reflector.

In the case of poststack migration, the data has already undergone a regularization process during stacking. Since poststack migration can be thought of as a process of spreading amplitudes over constant-traveltime surfaces (hemispheres in the constant velocity case), then it could potentially smooth out small-scale footprint that would be observed in a stack. However, if a strong footprint existed in the stack before migration, the amplitude variations would prevent the proper cancellation of migration wavefronts, resulting in footprint after poststack migration as well. Figure 14 shows that, compared to the stack differences from Figure 13, the footprint observed after poststack migration is somewhat less coherent; still, recognizable periodic amplitude variations remain,

producing percent variations of up to 6% on the featureless reflector and up to 5% at the channel level.

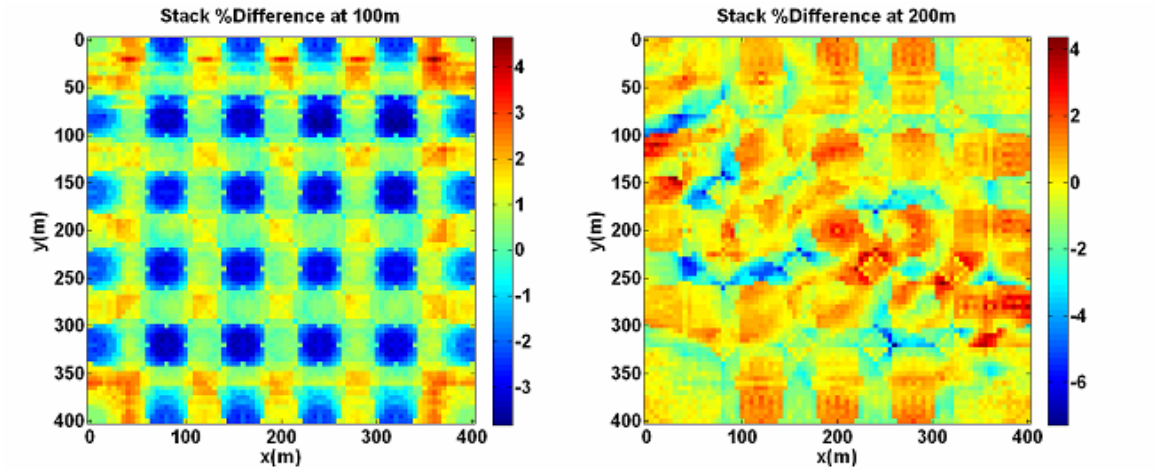

FIG. 13. Percent difference plots for stacks.

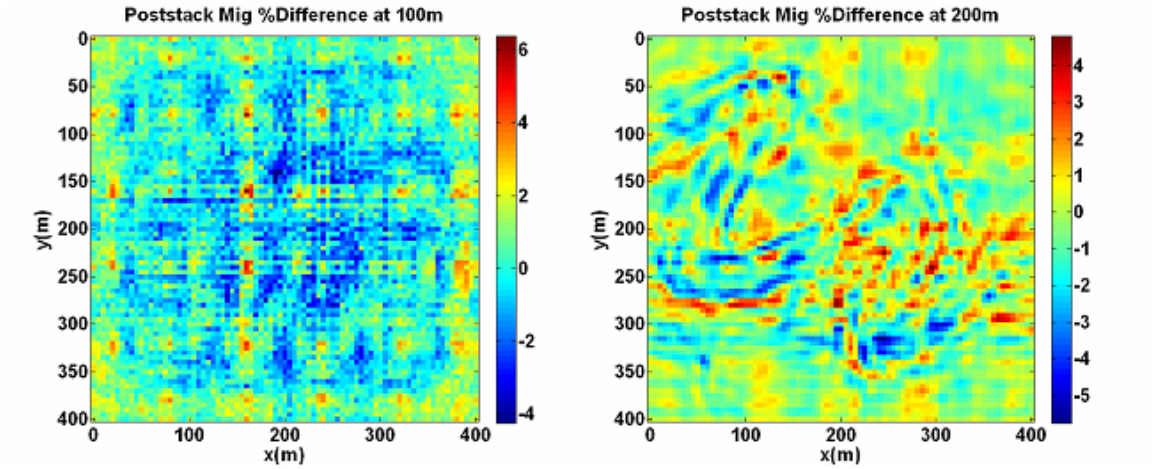

FIG. 14. Percent difference plots for poststack migrations.

In the prestack migration case, footprint may consist of residual migration wavefronts similar to those shown in the previous 2D simulations. The three algorithms used in this study show large differences in observable footprint, suggesting that migration weights and regularization methods are likely key to reducing the impact of poor sampling. The UofC algorithm, which does not involve any fold compensation methods, shows the largest percent amplitude variations: up to 24% on the featureless reflector and up to 17% at the channel (Figure 15). However, some of these differences are clearly not periodic; rather they are related to differences in the aperture effect of the exhaustive and decimated surveys. Our current measure used to quantify footprint is unable to separate the two types of variations. The prestack migrations performed using industry-standard algorithms show somewhat smaller amplitude variations: 7% variation on the featureless reflector and 8-14% variation on the channel reflector.

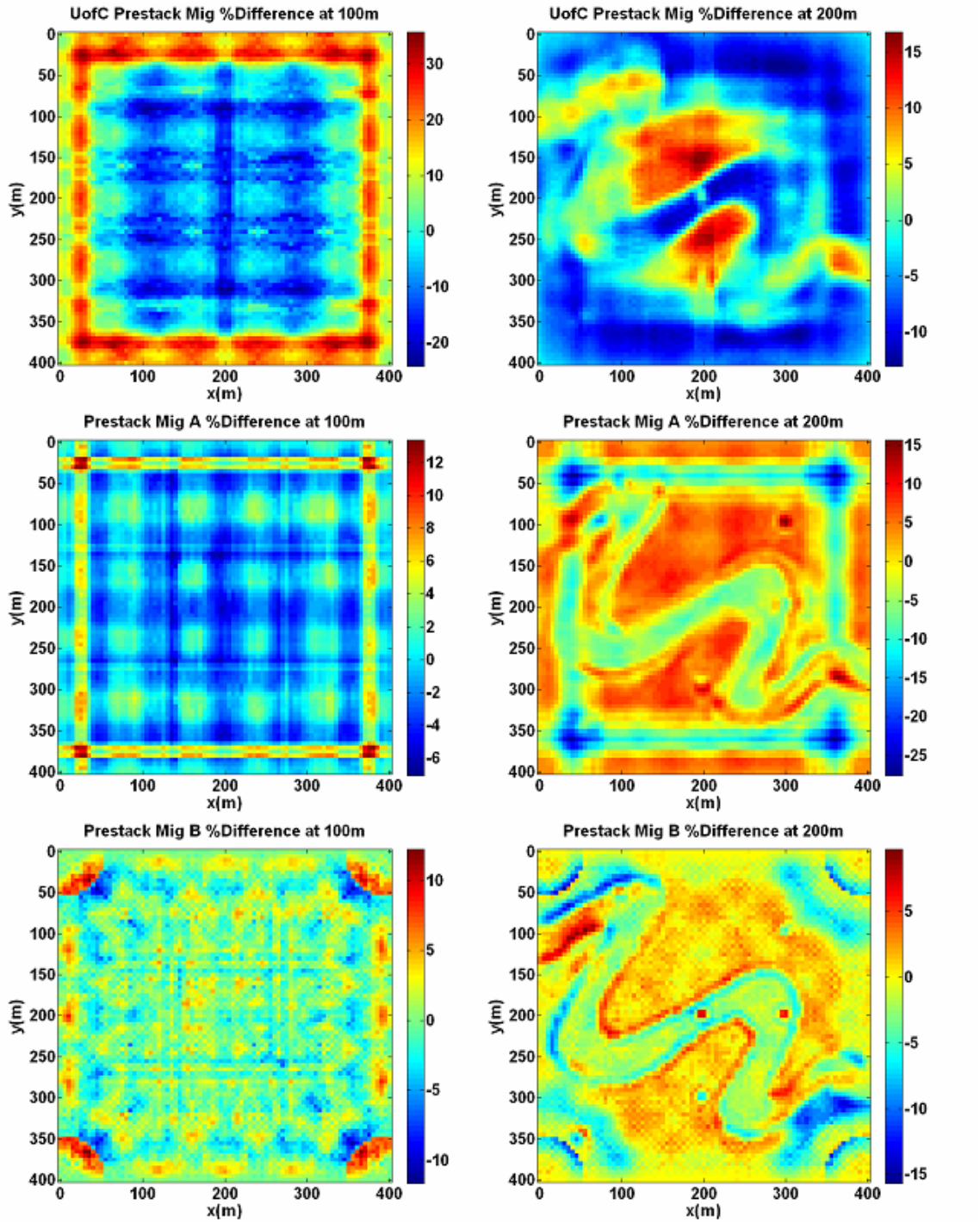

FIG. 15. Percent difference plots for prestack migrations at the shallow featureless reflector (left-hand column) and at the channel (right-hand column). Each row compares a particular migration algorithm run on the decimated dataset with the same algorithm run on the exhaustive dataset.

CONCLUSIONS

The objective of this project was to perform numerical simulations in order to investigate the causes of commonly observed artefacts in seismic field data, known as acquisition footprint. By defining footprint as any features observed on an image of a

featureless reflector, we consider two broad classes of footprint produced in this study. The first consists of amplitude variations related to the edges of the survey, including edge artefacts and aperture effects; this type of footprint was observed in both the exhaustive and decimated datasets, and was observed to vary between processing algorithms. The second class of footprint consists of amplitude variations in the interior of the survey; these variations we consider to be a product of inadequate spatial sampling that aliases the prestack wavefield. This premise is supported by the more prevalent occurrence of these artefacts in the decimated dataset. Observations of footprint in the decimated datasets are generally consistent with typical field data. In our simulations, observed footprint was (1) most severe after prestack migration, though highly variable using different prestack migration algorithms, (2) most organized in the unmigrated stack, and (3) somewhat randomized after poststack migration. Percent variations of up to 6% in stacked data, up to 6% in poststack migrated data, and up to 24% in prestack migrated data were observed. Future research will involve continued analysis and synthesis of the results from this project, in an attempt to make further generalizations about the causes of acquisition footprint. This research will involve the inclusion of additional complexities to the existing simulations, including larger, more intricate geologic models, more realistic survey designs (crooked lines, for example), and both coherent and random noise.

ACKNOWLEDGEMENTS

The majority of this research was conducted during the term of a MITACS Internship; we thank MITACS (Mathematics of Information Technology and Complex Systems) and Talisman Energy for financial support of this internship. Additional funding was provided by the industrial sponsors of CREWES, as well as by the Natural Sciences and Engineering Research Council of Canada (NSERC) and the Alberta Ingenuity Fund (AIF). We especially thank David D'Amico of Talisman Energy, Peter Cary and Rod Couzens of Sensor Geophysical, Mike Perz and Ye Zheng of Divestco, and Larry Mewhort and Ken Hedlin of Husky Energy for their helpful suggestions and considerable contributions to the project.

REFERENCES

Bancroft, J. C., 2006, A Practical Understanding of Pre- and Poststack Migrations: University of Calgary.

Bleistein, N., Cohen, J. K., and Stockwell, J. W., 2001, Mathematics of Multidimensional Seismic Imaging, Migration, and Inversion: Springer-Verlag New York, Inc.

Cary, P., 2007, 2-D Migration Footprint: CSEG Recorder, **32**, No. 6, 22-24.

Cordsen, A., Galbraith, M., and Peirce, J., 2000, Planning Land 3-D Seismic Surveys: Society of Exploration Geophysicists.

La Bella, G., Loinger, E., and Savini, L., 1998, The cross-shooting methodology: Design, acquisition, and processing: The Leading Edge, 17, 1549-1553.

Marfurt, K. J., Scheet, R. M., Sharp, J. A., and Harper, M. G., 1998, Suppression of the acquisition footprint for seismic sequence attribute mapping: Geophysics, **63**, 1024-1035.

Margrave, G. F., 2005, Footprint: A look at seismic acquisition geometries using 3D prestack depth migration: CREWES Research Report, **17**, 9.1-9.42.

Margrave, G. F. and Cooper, J. K., 2007, Seismic Modelling in 3D for Migration Testing: CREWES Research Report, this volume.

Shearer, P. M., 1999, Introduction to Seismology: Cambridge University Press.

Vermeer, G. J. O., 1990, Seismic Wavefield Sampling: Society of Exploration Geophysicists.

Vermeer, G. J. O., 1998, 3-D symmetric sampling: Geophysics, **63**, 1629-1647.